HHS Public Access

Author manuscript

Bone. Author manuscript; available in PMC 2016 December 01.

Published in final edited form as:

Bone. 2015 December ; 81: 593–601. doi:10.1016/j.bone.2015.09.007.

Non-Contact Strain Measurement in the Mouse Forearm Loading Model Using Digital Image Correlation (DIC)

Mark T. Begonia[a], **Mark Dallas**[b], **Bruno Vizcarra**[a], **Ying Liu**[b], **Mark L. Johnson**[b], and **Ganesh Thiagarajan**[a]

[a]University of Missouri-Kansas City, Department of Civil and Mechanical Engineering, 350K Robert H. Flarsheim Hall, 5110 Rockhill Road, Kansas City, MO 64110, USA

[b]University of Missouri-Kansas City, School of Dentistry, Department of Oral and Craniofacial Sciences, Room 3143, 650 E 25th Street, Kansas City, MO 64108, USA

Abstract

This study investigates the use of a non-contact method known as Digital Image Correlation (DIC) to measure strains in the mouse forearm during axial compressive loading. A two camera system was adapted to analyze the medial and lateral forearm displacements simultaneously, and the derived DIC strain measurements were compared to strain gage readings from both the ulna and radius. Factors such as region-of-interest (ROI) location, lens magnification, noise, and out-of-plane motion were examined to determine their influence on the DIC strain measurements. We confirmed that our DIC system can differentiate ROI locations since it detected higher average strains in the ulna compared to the radius and detected compressive strains on medial bone surfaces vs. tensile strains on lateral bone surfaces. Interestingly, the DIC method also captured heterogeneity in surface strain fields which are not detectable by strain gage based methods. A separate analysis of the noise intrinsic to the DIC system also revealed that the noise constituted less than 4.5% of all DIC strain measurements. Furthermore, finite element (FE) simulations of the forearm showed that out-of-plane motion was not a significant factor that influenced DIC measurements. Finally, we observed that average DIC strain measurements can be up to 1.5–2 times greater than average strain gage readings on the medial bone surfaces. These findings suggest that strain experienced in the mouse forearm model by loading is better captured through DIC as opposed to strain gages, which as a result of being glued to the bone surface artificially stiffen the bone and lead to an underestimation of the strain response.

Keywords

Strain; digital image correlation; forearm; ulna; radius

Corresponding Author: Ganesh Thiagarajan, University of Missouri-Kansas City, 350K Robert H. Flarsheim Hall, 5110 Rockhill Road, Kansas City, MO 64110, Phone: + 1 816 235 1288, ganesht@umkc.edu.

1. Introduction

During mechanical loading of bone, osteocytes have been hypothesized to be the initiators of cellular responses, in part through activation of the Wnt/β-catenin signaling pathway [1]. This process of mechanotransduction has been investigated in various studies [2–5]. Recent work has shown that compressive loading in the murine forearm activates Wnt/β-catenin signaling in three phases: (1) initial activation of a subpopulation of osteocytes at 1 hour post-loading, (2) subsequent activation of neighboring osteocytes, and (3) activation of osteoblasts on the bone surface at 24 hours post-loading [6]. Interestingly, the initial subpopulation of osteocytes activated in a heterogeneous pattern, suggesting localized differences in the strain field not captured in traditional finite element (FE) models and that osteocytes need to experience a minimum level of strain prior to activating in response to mechanical loading.

In order to study the strain distributions within the mouse forearm structure and their effects on osteocytes and bone function, a non-contact method for determining strain is needed. In a previous study [7], we developed a numerical FE model that included the ulna, radius, and the interosseous membrane and predicted the complete strain map along the forearm. However, the FE model must be biologically validated by comparing the numerical strain data against experimentally obtained data before the FE model can be used for further study with a wider range of boundary conditions. Strain gages can be applied successfully despite the small geometry of the mouse forearm (10–15 mm), but the resulting experimental data represents an average strain along a limited portion of the bone surface and does not offer insight regarding the localized strain field. Therefore, it is critical to seek an alternative approach that yields a more realistic strain measurement. The overall goal of this research is to develop a non-contact technique to study experimentally the distribution of strains on the mouse bone surface due to axial compressive loading. One technique for achieving this goal is using the Digital Image Correlation (DIC) method.

DIC is an optical, non-contact method of strain measurement that circumvents the limitations of strain gaging and can be used for biological validation of FE models. The DIC technique was proposed in the early 1980s [8–14] and has since been improved and widely used to measure the deformation and strain of various engineering materials and structures [15–21]. In the DIC procedure, a speckle pattern is first applied to the surface of a specimen. Cameras are then used to track the position of the speckle pattern while the specimen is loaded, and the ensuing sequence of images is processed using the DIC software. During the analysis, the field of view is divided into a region of interest (ROI) that measures the movement of the speckle pattern and subsequently calculates the displacement and strain [22, 23].

Various studies have demonstrated the merits of using DIC to examine different bone properties. Previous studies [24, 25] have utilized DIC to analyze micro cracks in bovine cortical bone to show that the crack tip locations and osteocyte lacunae produce the highest strains. DIC has also been used for comparing local strains with nanoindentation measurements in cortical bone to show that bone microstructure and mineral content affect local strain [26]. Although DIC has been employed in murine models involving the femur

[27] and the tibia [23, 28], to the authors' knowledge, this technique has not been employed on the forearm loading model. The DIC method has two major advantages over strain gages, namely that it is a non-contact measurement technique, and it can be used to quantify strains over the entire field of view using a post-processing technique, thereby capturing strain differences due to bone heterogeneity.

In the present study, we investigated the use of the DIC method to measure strains on the mouse forearm during axial compressive loading conditions. After developing a custom DIC system, we examined the effects of ROI location, lens magnification, noise, and out-of-plane motion on the strain magnitude. Strain measurements were obtained from both the ulna and radius through two methods: (1) strain gaging and (2) DIC. We determined that the DIC system was able to differentiate ROI locations and to distinguish between compression and tension on the medial and lateral bone surfaces, respectively. The DIC system detected a higher average strain magnitude in the ulna than the radius since the ulnar site experiences mechanical loading more directly. Lens magnification, noise, and out-of-plane motion did not significantly influence strains reported by the DIC system. Comparisons of DIC and strain gage measurements also revealed that DIC generally yielded a higher strain magnitude than conventional strain gaging. This finding suggests that a more realistic depiction of the forearm mechanical response can be captured through the DIC method, as strain gages underestimate strains due to the inherent stiffening caused by gluing the gages to the bone surfaces. This work ultimately demonstrates the benefits of utilizing DIC to capture the strain distribution in the mouse forearm subjected to axial compressive loading.

2. Materials and Methods

2.1 Equipment

The DIC system consisted of two digital single-lens reflex (DSLR) cameras and a loading system (Bose ElectroForce 3220, Bose Corp., ElectroForce Systems Group, Eden Prairie, MN). Both cameras (Canon REBEL T2i/EOS 550D) were equipped with MP-E 65 mm macro photo lenses (Canon U.S.A. Inc., Melville, NY), which have the capability of magnifications ranging from 1x to 5x using manual focusing. The camera was mounted to vertical adjustment columns bolted to an antivibration table and the system also included sliding rails, LED light sources, and external LCD monitors for optimizing video quality. Loading caps customized specifically for axial compression experiments were also installed in the Bose loading system (Supplemental Fig. 1).

2.2 *Ex Vivo* Mechanical Loading

This study employed the axial compression model for inducing mechanical deformation in the mouse forearm because it facilitates examination of mechanically induced bone formation in both rats and mice (Supplemental Fig. 2). In addition to mimicking physiological loading through the joints, this experimental model typically generates strains on the periosteal surface without damaging the surrounding soft tissue [29, 30]. For all experiments, the Bose system applied a preload of 0.3 N to forearm specimens and then dynamically loaded them to 2.25 N at a frequency of 0.2 Hz for 5 cycles using a Haversine waveform. A frequency of 0.2 Hz was chosen since it generated 150 data points for each

cycle (30 frames/sec x 5 sec/cycle). Based on our previous study [7], which examined the effect of loading frequency, the difference between the strain at 0.2 Hz and 2 Hz was ~1% in the ulna and ~6% in the radius after applying a preload of 0.3 N and a total load of 2 N.

Experimental strain measurements were obtained from strain gages (EA-06-015DJ-120/LE, Vishay Precision Group, Malvern, PA) attached to the medial forearm surface [31]. Strain gages were positioned approximately 2 mm distal to the midshaft on the ulna and radius (Supplemental Fig. 3). Each strain gage was trimmed down using a new razor blade under a binocular microscope. A multimeter was used to check the resistance before and after testing. After the muscle tissue was removed using microscissors and forceps, a cotton swab dipped in acetone was used to remove any remaining soft tissue from the bone. This step was taken to ensure that the gage adhered properly and tightly to the curved bone surfaces. Before the gage was attached, a small bead of glue was placed on the bone region. It should be noted that applying too much glue can yield strain results that characterize the properties of the glue rather than the bone underneath it. In addition, we did not use polyurethane coating because strain gages did not work properly after applying the coating in previous experiments. A cotton swab dipped in PBS was used to rehydrate the lateral bone surface prior to collecting strain data.

High-definition (HD) videos of loading and strain gage experiments were recorded at 30 frames per second. DIC was performed using videos of both loading and strain gage experiments in order to quantify the stiffening caused by application of strain gages to the bone surface. DIC strain values were obtained from DIC software that analyzed videos of experiments and then computed the strains. In order to further verify the strain predictions of the DIC method compared to strain gaging, we performed additional experiments to determine the load-strain relationship. The objective of these experiments was to determine the relationship between the load applied and the strain measured for both strain gaging and the DIC method. The Bose system applied the same preload, frequency, and number of cycles. However, experiments were performed on each forearm specimen at different peak loads, which ranged from 1.25 N to 3.25 N at increments of 0.25 N.

2.3 Specimen Preparation

Female TOPGAL mice (age 17.5 to 19.5 weeks) were selected for this research as they will be used specifically to detect the activation of the β-catenin signaling pathway in future experiments correlating cellular activation with strain [32]. These mice were maintained in our colony on a mixed C57Bl/6 X CD1 background. Mice were euthanized, the skin from the forelimb removed, and muscle tissue was removed from the radius and ulna. The paw and olecranon remained intact to recreate physiological loading conditions and to facilitate forearm positioning between the loading caps of the Bose lading system. A cotton swab dipped in PBS was used to keep the forearm specimens hydrated throughout preparation. Forearm specimens were then wrapped in gauze soaked with PBS and stored in a −20°C freezer.

Prior to testing, forearm specimens were thawed for 30 minutes, rehydrated with PBS, and then speckled with black, opaque, water-based paint (Createx Colors, East Granby, CT) using a high precision airbrush (Model 200NH, Badger Air-Brush Co., Franklin Park, IL) set

to a pressure of 138 kPa (20 psi). To generate a consistent speckle pattern, we mounted the airbrush at a height of 15.25 cm (6 in.) and distance of 30.5 cm (12 in.) from the specimen and then inclined it at a 45° angle. The speckling process consisted of four air bursts onto the medial side of the forearm followed by four air bursts onto the lateral side. This speckling process is similar to the speckling procedure described in a previous work that used DIC to analyze the strain distributions during mechanical loading of the mouse tibia [33].

2.4 Digital Image Correlation (DIC)

Numerous methods are available for digital image processing and tracking embedded image features. Each method utilizes a specific algorithm that may be ideal for certain applications [16, 22]. We used the two-dimensional digital image correlation (2D-DIC) technique and analyzed images with sub-pixel resolution. Typically, the 2D-DIC method measures the displacement vector acting on an image stack and then calculates the corresponding strains. For this study, we used DIC code [36–38] developed in MATLAB® (MathWorks, Inc., Natick, MA). In general, the region of interest (ROI) selected for analysis is first divided into grid points. Each grid point is represented by a subset of 11×11 pixels that surround it. The pixel intensities of these 11×11 pixels are then searched for and compared to the pixel intensities in a 40×40 region around the original grid point in the next video frame. The DIC code then calculates a correlation coefficient for each search, and the new 11×11 pixel subset that gives the highest correlation coefficient is identified as the new grid point in the next video frame. This process continues until the final video frame is analyzed, and the first frame of the video is always selected as the reference frame. The displacement map for each grid point is then generated as a matrix of values. These displacements are then smoothed using the Savitzky-Golay (SG) filter [18] and the corresponding strain values are calculated using basic kinematic equations, which are built into the DIC code.

Modifications to the original code developed by Jones et al. (2014) included the addition of the SG filter at the displacement level and the development of the optimal frame size number. Since strain magnitudes are derived from displacement data, smoothing the displacements results in smoother strain magnitudes. The SG filter is based on a local least squares approximation of the data while maintaining the height and shape of the overall data set. One of the parameters required for this filtering operation is the number of successive frames to be considered for the smoothing process. After conducting various trials, we found that a frame size number of 159 was optimal for smoothing data between two consecutive video frames.

Both DSLR cameras captured full HD videos (1920 × 1080 pixel resolution) that were approximately 90 seconds in length. HD videos of forearm loading experiments were acquired at 30 frames per second using a shutter speed of 1/60 seconds. These camera settings allowed the DIC code to analyze 150 data points for each loading cycle. In addition, multiple magnifications (2x, 3x, and 4x) were selected for use with the MP-E 65 mm macro photo lens in order to determine the sensitivity of the DIC system to changes in magnification and to determine an ideal magnification for future studies.

Prior to testing, cameras were placed in the medial and lateral viewing positions (Supplemental Fig. 1). Each forearm specimen was then secured between the loading caps while the macro photo lenses were set to the 4x magnification. Sliding rails and external LCD monitors were used for optimizing video resolution of the speckled bone surfaces. The forearm specimen was also rotated to ensure that both the ulna and radius remained in focus. Both cameras were synchronized to record videos simultaneously, but activation of the Bose loading system was intentionally delayed for 60 seconds. This delay allowed the camera vibration to subside after manual triggering and also allowed a sufficient number of static frames to be recorded (60 sec × 30 frames/sec = 1800 frames) for analysis of the inherent noise of the DIC system. Consequently, each test started after 60 seconds had passed, and this procedure was repeated for the 3x and 2x magnifications.

Video footage was separated into individual frames using a custom MATLAB® script, and frames were divided into two subsets that corresponded to either non-loading (i.e. static) or loading (i.e. dynamic) conditions. These designations were determined by inspection through a movie viewing program immediately following video acquisition. Static frames were analyzed to quantify the strain due to noise from the DIC system while dynamic frames were analyzed to measure the strains corresponding to cyclic loading only. Although the test protocol applied 5 cycles, the peak-to-peak strain was averaged from the second, third, and fourth cycles (Fig. 1). Figures 1(A) and 1(B) show representative plots of the strain history after performing DIC on the lateral radius and medial radius, respectively, at 3 different lens magnifications. For this study, the DIC strain magnitudes are defined as the difference between the peak-to-peak strain and the strain due to noise since identical ROIs were selected for DIC of both dynamic and static frames.

ROI dimensions were matched to the sensing area of the strain gage (510 μm × 380 μm) rather than its entire surface area (5.8 mm × 3.0 mm) because the sensing area is the only region on the strain gage that collects strain data directly from the bone surface. Since multiple lens magnifications were utilized, ROI dimensions were adjusted accordingly using the scaling options in ImageJ (National Institutes of Health, Bethesda, MD) [39, 40]. The resolutions for ROIs at the 2x, 3x, and 4x magnifications were 86 × 64 pixels, 144 × 96 pixels, and 172 × 128 pixels, respectively. In addition, we chose a subset size of 40 × 40 pixels and step size of 10 pixels for this study. The subset size defines the region whose pixel features are chosen for comparison, and the step size represents the distance (in pixels) that this region can move between two successive frames. During the determination of the displacement, the pixel intensities in a region of 11×11 is considered to represent a grid point. The search window for the new location of this region is 40×40 pixels. These two values were based on a separate parametric analysis that determined the effects of both subset size and step size on DIC strain measurements. All ROIs were located along the midshaft of both the ulna and radius, and their positions remained consistent across all three magnifications. This procedure for designating ROIs facilitated a direct comparison of DIC and strain gage measurements as well as DIC strains across different magnifications.

2.5 Out-of-Plane Motion

The two-dimensional DIC technique can be influenced by deformations that occur toward and away from the camera's field of view (i.e. out-of-plane motion), especially when a specimen with a complex geometry is analyzed. To investigate the out-of-plane motion induced, we created a 3D finite element (FE) model of the TOPGAL mouse forearm and a loading cap positioned over the distal end. Mimics® 8.0 and 3-matic® 16.0 (Mimics Innovation Suite, Materialise, Plymouth, MI) were used to generate a volume mesh consisting of 10-noded tetrahedral elements. The FEBio Software Suite (Musculoskeletal Research Laboratories, Salt Lake City, UT) [41] was used to simulate one loading cycle. In the FE model, the z-axis coincided with the longitudinal axis of the forearm and the direction of the applied load. At the midshaft of each bone, the displacement along the y-axis corresponded to the out-of-plane deformation.

A separate *ex vivo* loading experiment was performed on a comparable specimen (i.e. TOPGAL, female, 20 weeks old) by rotating the forearm 90 degrees relative to the original orientation and then capturing the out of plane deformation via DIC (Fig. 8). ROIs along the midshaft of the ulna and radius were analyzed to calculate the out-of-plane displacement. This additional experiment was performed because the numerical displacements from the FE model may differ due to simplifications in the geometry (e.g. absence of soft tissue and paw).

2.6 Statistical Analysis

One-way analysis of variance (ANOVA) was performed at each ROI to identify significant differences in DIC strain measurements based on the lens magnification selected. The assumption of equal variances between groups was investigated with Levene's test. Based on the Levene's test result, different approaches were applied to post-hoc multiple comparisons. More specifically, to keep the nominal level of type I error rate, Tukey's HSD test was used for equal variances while Dunnett's T3 was used for unequal variances. For the medial ulna and medial radius, independent samples t-tests were used to identify any significant differences between strain gage and DIC values. Similarly, Levene's test was used to confirm the assumption of equal variance. Data analysis was performed with SPSS (Statistical Package for Social Science, version 22; IBM SPSS Inc., Chicago, IL), and $p<0.05$ was considered significant.

3. Results

Figures 2(A) and 2(B) show representative strain contour plots after performing DIC on the lateral ulna and medial ulna, respectively. A larger ROI was selected to better illustrate the non-uniform strain response on the ulna surface during mechanical loading. For this study, however, DIC strain measurements were obtained from smaller ROIs (510 μm × 380 μm) that corresponded to the dimensions of the strain gage sensing area, thus allowing a more direct comparison between DIC and strain gage values.

Figure 3 shows the load-strain relationships after performing strain gaging and DIC on the medial ulnas of the same set of forearms (n=4). We assigned a reference microstrain value at 0.3 N in order to calculate the strain due to the cyclic loading from 0.3 N to 2.25 N. This

reference point was added to facilitate a more direct comparison of the two slopes in Figure 3 since the two regression lines have the initial condition of zero strain at a preload of 0.3 N. Although both load-strain relationships were linear, DIC exhibited a 24% stiffer slope compared to strain gaging. The lower slope for the strain gage load-strain plot is most likely due to a stiffer response caused by gluing strain gages to the bone surface. Meanwhile, the higher slope observed in the DIC load-strain plot could be attributed to the uninhibited movement of the forearm during loading.

Figure 4 shows a comparison of the average peak-to-peak strains (Mean ± SD) after strain gaging the medial surfaces of the ulna and radius. The sample sizes for the experimental strains of the ulna (n=5) and radius (n=3) reflect the number of forearm specimens. Since strain gage measurements were collected while testing at each lens magnification, each forearm yielded 3 separate gage readings. Therefore, the experimental strains for the ulna and radius were averaged from 9 and 15 gage readings, respectively. The variability over the repeated readings in each bone was relatively small. The variability for the 5 ulna samples was 20 με, 24 με, 52 με, 75 με, and 4 με whereas the variability for the 3 radius samples was 26 με, 54 με, and 43 με. As shown in Figure 4, the experimental strains were 77% higher in the ulna compared to the radius.

Figure 5 shows the DIC strain measurements obtained from different ROI locations and lens magnifications. The negative DIC strain values for the medial ROIs and the positive DIC strain values for the lateral ROIs indicate that the DIC system is sensitive to variations in the ROI location. Figure 5 also shows a range of DIC strain measurements that could be attributed to differences in magnification. Since a higher magnification leads to a higher ROI resolution and hence a higher sensitivity to measuring the displacements, we anticipated a rise in the average DIC strain values as the magnification increased from 2x to 4x. In addition, one-way ANOVA was performed to confirm that the DIC strains were not significantly different due to changes in magnification.

Figure 6 compares strain gage and DIC values for the medial ulna and medial radius at magnifications of (A) 2x, (B) 3x, and (C) 4x. At all three magnifications, DIC detected significant increases in strain compared to gage readings. For instance, the average DIC strains for the medial ulna were 1.8, 2.0, and 2.1 times higher than the corresponding gage readings at 2x, 3x, and 4x, respectively. Similarly, the average DIC values for the medial radius were 2.5, 2.9, and 3.1 times higher compared to the gage values at 2x, 3x, and 4x, respectively.

Despite its advantages over traditional strain gaging, the 2D-DIC method can be influenced by factors such as noise and out-of-plane motion. Table 1 shows the average noise detected within the DIC system and how much it contributes to the DIC strain measurements on the forearm surface. Estimated noise ranges were 46–79 με in the lateral radius, 53–93 με in the lateral ulna, 68–110 με in the medial radius, and 70–92 με in the medial ulna. The noise level did not vary substantially based on the ROI location or the magnification selected. More importantly, these results indicate that noise constituted less than 4.5% of all DIC strain measurements. After quantifying the noise within the DIC system, we also developed a finite element model of the mouse forearm to approximate the out-of-plane motion (i.e.

bone deformations toward and away from the focal plane of the camera). The FE model exhibited out-of-plane displacements of approximately 80 μm in the ulna midshaft and 40 μm in the radius midshaft (Supplemental Fig. 4). After performing DIC on a reoriented forearm specimen, we found that the out-of-plane displacements were approximately 7 μm for the ulna and 54 μm for the radius.

4. Discussion and Conclusions

4.1 Ulna and Radius Comparison

We found that experimental strains were 77% higher in the ulna compared to the radius (Figure 4). The significant difference in strains between these two bones highlights the need for characterizing the mechanical response of both the ulna and radius. The merits of assigning separate mechanical properties to each forearm bone has been shown in a previous work that compared numerical results between an ulna-only forearm model (UM) and an ulna-radius forearm model (URM) [42]. The radius proved to be more challenging in terms of not only attaching the strain gages but also collecting reliable data, (only 3 of 5 radii tested gave usable data). We believe that the curvature and limited contact surface of the radius in a few samples prevented proper adhesion of the strain gage sensing region and resulted in the gages not working properly during the testing phase. However, the gage readings that were successfully collected from the radius should provide a basis of comparison for other investigators who may be interested in characterizing the strain response of the radius under mechanical loading.

4.2 Strain Gage Stiffness Effect

In the mouse forearm loading model, wrist flexion causes the medial bone surfaces to experience compression whereas the lateral bones surfaces experience tension. The presence of a strain gage on the medial surface would inhibit bone deformation on the medial side and, in turn, on the lateral side of the forearm as well. Any large decreases in strain could be attributed to this altered mechanical loading of the forearm as well as the irregular geometries and heterogeneous properties of the bones themselves. Figure 7 compares the third loading cycle in forearms (n=5) before and after strain gages were attached to the bone surface. For each forearm, we observed a stiffer mechanical response as evidenced by a decrease in displacement despite identical load amplitudes. Bone deformations were quantified by calculating the stiffness (i.e. slope) of the unloading curves. We found that after gages were applied, the stiffness values increased by a factor of 1.2 – 2.3 (Table 2). These results coincide with the strain gage vs. DIC comparisons (Fig. 6), which suggest that gluing strain gages onto the bone surface leads to an artificially stiffer mechanical response.

4.3 Strain Gage and DIC Comparison

Although strain gages have been used traditionally for measuring the strain response in mouse bones, DIC is a method with benefits that include non-contact measurement and enhanced resolution. Another important advantage of the DIC approach is the ability to measure strains across the entire bone surface, whereas strain gage positioning is limited by the surface available for gluing the gage. Furthermore, the strain response is better captured through DIC versus strain gaging, which can underestimate the true strain values due to an

artificial stiffening caused by gluing strain gages to the bone surface. The objective of this study was to quantify this underestimation in bone surface strains by comparing DIC strain measurements with strain gage readings. We observed that the average DIC strain values exceeded the corresponding average gage values by a factor of 1.8 – 2.1 in the medial ulna and by a factor of 2.5 – 3.1 in the medial radius (Fig. 6). These differences in strain suggest that DIC better characterizes the strain response in the mouse forearm loading model compared to conventional strain gaging.

Since only black paint was applied in the current study, we believe that the speckling process did not alter bone surface properties or only led to a minimal change. It is also possible for DIC strain measurements to vary with different sets of speckle coating, but we removed this confounding factor by utilizing a high precision airbrush to standardize the speckling procedure. Previous studies have suggested applying a printed speckle pattern to the bone surface, but this technique would be difficult due to the size and geometry of mouse bones [34, 35]. As recommended by [28], the best way to control the speckle size and to apply a consistent pattern is to use a high precision airbrush. Although changes in water content could also alter the mechanical properties of bone, we prepared all samples in the same manner and believe that any reduction in water content should be similar between specimens.

4.4 ROI Location Effect

Figure 5 shows that DIC strain measurements were strongly influenced by variations in the ROI location. We found that the DIC code reported positive strains for the lateral ROIs and negative strains for the medial ROIs. This finding is important because it verifies that the DIC system is capable of differentiating strain responses based on the ROI assigned. Furthermore, the sign conventions are consistent with the axial compression loading model because wrist flexion during mechanical loading causes the medial surfaces of the radius and ulna to experience compression while the lateral bone surfaces experience tension.

As shown in Figure 2, both the lateral and medial surfaces can experience a mixture of tension and compression due to the heterogeneous properties of bone. A similar behavior was observed by Hein [33] after performing DIC of the mouse tibia. Since the strain contours are displayed at approximately 1/8 of a loading cycle, Figure 2 shows more clearly a mixture of tension and compression. At the end of a full loading cycle (2.25 N), however, the full strain contour coincides with either a predominantly tensile response (i.e. varying shades of red) for the lateral ulna surface or a predominantly compressive response (i.e. varying shades of blue) for the medial ulna surface (Supplemental Fig. 5).

4.5 Lens Magnification Effect

A rise in the average DIC strain values was anticipated for all 4 ROIs as the magnification increased from 2x to 4x. In general, a higher magnification leads to greater image resolution and thus a larger number of pixels that constitute a particular ROI. For instance, the length of the sensing grid on the strain gage is 510 μm, but the number of pixels used to represent this distance is different for each magnification. At 2x, 3x, and 4x, a distance of 510 μm corresponds to 86, 144, and 172 pixels, respectively. There are also differences in the

number of pixels needed to represent the width of the sensing grid (380 μm) at each magnification. Hence, the ROIs used for strain measurements at 2x, 3x, and 4x are 86 × 64, 144 × 96, and 172 × 128 pixels, respectively. Since each ROI comprises a different number of pixels at each magnification, it is possible for a higher magnification to capture a slightly higher strain due to the increased image resolution.

For most cases, the average DIC strain measurements increased in conjunction with a higher lens magnification (Fig. 5), but these changes in strain were not significant (Table 3). Interestingly, the lateral ulna showed a 5% lower DIC strain (p=0.893) as the magnification changed to 3x followed by a 6% lower DIC strain (p=0.999) as the magnification changed to 4x. These decreases in strain with increasing magnification suggest that the DIC system was able to capture the strain response at all 3 magnifications in the lateral ulna. In addition, the lateral radius exhibited average DIC strain measurements that were higher than those of the lateral ulna at 3x (~21%) and 4x (~32%). The increased DIC strain values observed in the lateral radius could be attributed to two factors. First, forearms without strain gages glued to the surface would allow the radius to bend more freely during loading, subsequently generating higher DIC strain values along the surface of the radius. Second, the ulna may not always carry the majority of the mechanical load during forearm testing [30]. Consequently, load sharing between the radius and ulna may occur through other forearm structures such as the interosseous membrane [7, 43], which remained intact in all forearm specimens. In summary, we determined that the DIC strain measurements were not significantly influenced by changes in lens magnification.

4.6 Noise Effect

When assessing other factors that could diminish the accuracy of the DIC strain measurements, we determined that noise could be an issue due to sources of vibration (e.g. laboratory floor and HVAC system). Consequently, adjustment columns and an antivibration table were incorporated into the DIC system to further stabilize the DSLR cameras during testing, thus minimizing the potential noise. As shown previously in Table 1, the noise observed at each ROI and lens magnification never exceeded 4.5% of the total strain. Therefore, noise was not believed to be a major contributing factor in the measurements of strain using DIC.

4.7 Out-of-Plane Motion Effect

Although 2D-DIC is supposedly limited to capturing strains in planar specimens [16, 22], this study shows that this technique can be effective at measuring strains on complex, non-planar specimens such as bone. DIC strain measurements on the forearm were assumed to be minimally affected by out-of-plane motion since loss of focus was not observed at 2x, 3x, or 4x magnification during testing. In addition, differences between DIC and strain gage values could be associated with inherent biological factors (e.g. bone curvature and surface texture) as well as experimental factors (e.g. forearm positioning and lateral bone deformation). When comparing results from the FE model and DIC of the reoriented forearm, we found that out-of-plane displacements varied by 73 μm in the ulna midshaft and 14 μm in the radius midshaft. One possible explanation for the differences between the FE and DIC out-of-plane deformations could be the simplified geometry of the FE model, which did not

include the paw and subsequently may have slightly altered the load distribution through the two bones. Based on these results, we believe that out-of-plane motion did not have a major influence on the on the variability of the DIC strain measurements.

4.8 Limitations and Concluding Remarks

This study highlights the benefits of the DIC method over traditional strain gaging, but each technique has its limitations. When strain gaging mouse bones, especially forearms, it can be difficult not only to attach the gages but also to collect reliable data. This was evidenced by the reduced sample sizes for the radius (n=3) versus the ulna (n=5) due to a failure to obtain reliable data in 2 of the 5 radii tested. We attribute this to poor adhesion of the strain gage sensing region, which could be due to the limited contact surface and curvature of the radius. For the 2D-DIC method, it is important that the deformations are low and stay as close to in-plane as possible. If bone deformations are excessive due to out-of-plane motion, then the 3D-DIC technique must be employed. Another factor to consider is the time and expense required to build an appropriate DIC system that includes features such as multiple cameras, custom fixtures for the loading device, and software. Additional components may also be necessary to facilitate smoother performance of DIC experiments. Two examples include an antivibration table for minimizing environmental noise from laboratory floors and HVAC systems as well as repurposed microscope bases that allow both vertical and horizontal camera adjustment. Furthermore, when applying DIC to bones it is important to collect a sufficient number of specimens to perform an appropriate load-strain analysis followed by the actual loading experiments. This factor is especially critical since specific loading regimens made be needed for different mice in order to elicit a predetermined strain response and then correlate it with variables such as age, gender, bone, or genetic background. Lastly, the current study analyzed forearms that were collected from mice with up to a 2-week difference in age. These mice were past the peak bone growth phase and we did not anticipate the bone development to vary substantially over this period, but this age range nonetheless may have contributed to some variability in the strain measurements.

Although our lens is capable of magnifications of 1x-5x, we decided not to use the extremes of 1x and 5x in the current study. We did not utilize the 1x magnification because the bone size was relatively small in relation to the field of view. We also did not use the 5x magnification because the field of view eliminated other bone regions (i.e. distal and proximal ends of the forearm) from being analyzed through DIC. Therefore, we decided to proceed with 2x-4x in our DIC experiments. Since we did not know initially which magnification would be optimal for DIC of the mouse forearm, we incorporated this variable into the current study. Ultimately, we believe that 3x provides the best option for DIC system in this study due to the wider field of view and higher signal-to-noise ratio (SNR) compared to 4x and 2x, respectively.

From an experimental standpoint, the DIC method can be adapted to analyze a variety of bones provided that out-of-plane motion is minimal and strain gage readings are available for comparison. The full strain field obtained from DIC can also provide insight on the strain distributions in regions away from the typical strain gage location, which is usually the midshaft of the bone. Strain analysis of regions closer to the proximal and distal ends of the

bone are achievable through DIC yet challenging via strain gaging due to the limited bone surface area available for attaching the strain gages. More importantly, the full strain field obtained through DIC would be especially useful for biologically validating finite element (FE) models since DIC captures localized strain fields that are more likely to correlate with the heterogeneous properties of bone; whereas strain gages only capture a spatial average of the strain over a restricted region.

In this study, we devised a system for non-contact strain measurement of the TOPGAL mouse forearm undergoing axial compression. We then utilized strain gages and DIC to analyze strains on the bone surfaces of both the ulna and radius. Strain gage and DIC measurements confirmed that ROI location alters the peak-to-peak strain response. Meanwhile, factors such as lens magnification and noise did not significantly change the DIC strain values. The out-of-plane deformations for the ulna and radius, which were determined through both FE modeling and DIC, indicated that the DIC results were not strongly influenced by out-of-plane motion. DIC is not only a viable non-contact method of strain measurement, but this technique also facilitates a wider range of analytical capabilities that cannot be achieved using strain gages (e.g. multiple ROI locations, variable ROI dimensions, multidimensional strain contours). Most importantly, however, this study suggests that better representations of the strain response can be achieved through DIC rather than strain gages, which most likely underestimate strains due to the artificially stiffer response caused by their attachment to the bone surface. Future work will utilize this DIC system to conduct studies designed to examine strain differences based on gender and age. Our ultimate goal is to use the bone surface strain mapping to investigate if the heterogeneous activation of Wnt/β-catenin signaling is predominantly influenced by a minimum strain threshold or osteocyte mechanosensitivity that progressively worsens with aging.

Supplementary Material

Refer to Web version on PubMed Central for supplementary material.

Acknowledgments

This work was funded by a grant from the National Institutes of Health – NIA P01 AG039355 (LF Bonewald-PI) and NIAMS R01 AR053949 (ML Johnson – PI). The authors also wish to thank Dr. Lynda Bonewald for her critical review of this manuscript as well as Dr. Dan Nicolella for his insightful commentary.

References

1. Bonewald LF, Johnson ML. Osteocytes, mechanosensing and Wnt signaling. Bone. 2008; 42:606–615. [PubMed: 18280232]
2. Robinson JA, Chatterjee-Kishore M, Yaworsky PJ, Cullen DM, Zhao W, Li C, Kharode Y, Sauter L, Babij P, Brown EL, Hill AA, Akhter MP, Johnson ML, Recker RR, Komm BS, Bex FJ. Wnt/β-Catenin signaling is a normal physiological response to mechanical loading in bone. Journal of Biological Chemistry. 2006; 281:31720–31728. [PubMed: 16908522]
3. Lau K-HW, Kapur S, Kesavan C, Baylink DJ. Up-regulation of the Wnt, estrogen receptor, insulin-like growth Factor-I, and bone morphogenetic protein pathways in C57BL/6J osteoblasts as opposed to C3H/HeJ osteoblasts in part contributes to the differential anabolic response to fluid shear. Journal of Biological Chemistry. 2006; 281:9576–9588. [PubMed: 16461770]

4. Sawakami K, Robling AG, Ai M, Pitner ND, Liu D, Warden SJ, Li J, Maye P, Rowe DW, Duncan RL, Warman ML, Turner CH. The Wnt co-receptor LRP5 is essential for skeletal mechanotransduction but not for the anabolic bone response to parathyroid hormone treatment. Journal of Biological Chemistry. 2006; 281:23698–23711. [PubMed: 16790443]
5. Robling AG, Niziolek PJ, Baldridge LA, Condon KW, Allen MR, Alam I, Mantila SM, Gluhak-Heinrich J, Bellido TM, Harris SE, Turner CH. Mechanical stimulation of bone in vivo reduces osteocyte expression of Sost/sclerostin. Journal of Biological Chemistry. 2008; 283:5866–5875. [PubMed: 18089564]
6. Lara-Castillo N, Kim NA, Kamel MA, Javaheri B, Ellies D, Krumlauf R, Thiagarajan G, Johnson ML. In vivo mechanical loading rapidly activates β–catenin signaling in osteocytes through a prostaglandin mediated mechanism. Bone. 2015 Under Second Review.
7. Thiagarajan G, Lu Y, Dallas M, Johnson ML. Experimental and finite element analysis of dynamic loading of the mouse forearm. Journal of Orthopaedic Research. 2014; 32:1580–1588. [PubMed: 25196694]
8. Peters WH, Ranson WF. Digital Imaging Techniques In Experimental Stress Analysis. Optical Engineering. 1982; 21:213427–213427.
9. Peters WH, Ranson WF, Sutton MA, Chu TC, Anderson J. Application Of Digital Correlation Methods To Rigid Body Mechanics. Optical Engineering. 1983; 22:226738–226738.
10. Sutton MA, Wolters WJ, Peters WH, Ranson WF, McNeill SR. Determination of displacements using an improved digital correlation method. Image and Vision Computing. 1983; 1:133–139.
11. Chu TC, Ranson WF, Sutton MA. Applications of digital-image-correlation techniques to experimental mechanics. Experimental Mechanics. 1985; 25:232–244.
12. Sutton MA, Mingqi C, Peters WH, Chao YJ, McNeill SR. Application of an optimized digital correlation method to planar deformation analysis. Image and Vision Computing. 1986; 4:143–150.
13. Sutton MA, McNeill SR, Jang J, Babai M. Effects Of Subpixel Image Restoration On Digital Correlation Error Estimates. Optical Engineering. 1988; 27:271070–271070.
14. Bruck HA, McNeill SR, Sutton MA, Peters WH III. Digital image correlation using Newton-Raphson method of partial differential correction. Experimental Mechanics. 1989; 29:261–267.
15. Cofaru C, Philips W, Van Paepegem W. Improved Newton-Raphson digital image correlation method for full-field displacement and strain calculation. Appl Opt. 2010; 49:6472–84. [PubMed: 21102673]
16. Pan B, Qian K, Xie H, Asundi A. Two-dimensional digital image correlation for in-plane displacement and strain measurement: a review. Measurement science and technology. 2009; 20:062001.
17. Pan B, Wang Z, Xie H. Generalized spatial-gradient-based digital image correlation for displacement and shape measurement with subpixel accuracy. The Journal of Strain Analysis for Engineering Design. 2009; 44:659–669.
18. Pan B, Xie H, Guo Z, Hua T. Full-field strain measurement using a two-dimensional Savitzky-Golay digital differentiator in digital image correlation. Optical Engineering. 2007; 46:033601–10.
19. Tiwari V, Sutton MA, McNeill SR. Assessment of High Speed Imaging Systems for 2D and 3D Deformation Measurements: Methodology Development and Validation. Experimental Mechanics. 2007; 47:561–579.
20. Wang Y, Cuitiño AM. Full-field measurements of heterogeneous deformation patterns on polymeric foams using digital image correlation. International Journal of Solids and Structures. 2002; 39:3777–3796.
21. Zhou P, Goodson K. Subpixel displacement and deformation gradient measurement using digital image/speckle correlation (DISC). Optical Engineering. 2001; 40:1613–1620.
22. Sutton, M.; Orteu, J.; Schreier, H. Image Correlation for Shape, Motion and Deformation Measurements. Springer; US: 2009.
23. Sztefek P, Vanleene M, Olsson R, Collinson R, Pitsillides AA, Shefelbine S. Using digital image correlation to determine bone surface strains during loading and after adaptation of the mouse tibia. Journal of Biomechanics. 2010; 43:599–605. [PubMed: 20005517]

24. Nicolella DP, Nicholls AE, Lankford J, Davy DT. Machine vision photogrammetry: a technique for measurement of microstructural strain in cortical bone. Journal of Biomechanics. 2001; 34:135–139. [PubMed: 11425075]
25. Nicolella DP, Moravits DE, Gale AM, Bonewald LF, Lankford J. Osteocyte lacunae tissue strain in cortical bone. Journal of Biomechanics. 2006; 39:1735–1743. [PubMed: 15993413]
26. Hoc T, Henry L, Verdier M, Aubry D, Sedel L, Meunier A. Effect of microstructure on the mechanical properties of Haversian cortical bone. Bone. 2006; 38:466–474. [PubMed: 16332459]
27. Yang L, Zhang P, Liu S, Samala PR, Su M, Yokota H. Measurement of strain distributions in mouse femora with 3D-digital speckle pattern interferometry. Optics and lasers in engineering. 2007; 45:843–851. [PubMed: 18670581]
28. Carriero A, Abela L, Pitsillides AA, Shefelbine SJ. Ex vivo determination of bone tissue strains for an in vivo mouse tibial loading model. J Biomech. 2014; 47:2490–7. [PubMed: 24835472]
29. Torrance A, Mosley J, Suswillo R, Lanyon L. Noninvasive loading of the rat ulna in vivo induces a strain-related modeling response uncomplicated by trauma or periostal pressure. Calcified Tissue International. 1994; 54:241–247. [PubMed: 8055374]
30. McBride SH, Silva MJ. Adaptive and Injury Response of Bone to Mechanical Loading. Bonekey Osteovision. 2012:1.
31. Robling AG, Li J, Shultz KL, Beamer WG, Turner CH. Evidence for a skeletal mechanosensitivity gene on mouse chromosome 4. The FASEB Journal. 2003; 17:324–326. [PubMed: 12490544]
32. DasGupta R, Fuchs E. Multiple roles for activated LEF/TCF transcription complexes during hair follicle development and differentiation. Development. 1999; 126:4557–4568. [PubMed: 10498690]
33. Hein JM. Ultrasonic and Stereo-Optical Characterization Techniques for Applications in Mechanical Testing. 2011
34. Lecompte D, Smits A, Bossuyt S, Sol H, Vantomme J, Van Hemelrijck D, Habraken A. Quality assessment of speckle patterns for digital image correlation. Optics and lasers in Engineering. 2006; 44:1132–1145.
35. Haddadi H, Belhabib S. Use of rigid-body motion for the investigation and estimation of the measurement errors related to digital image correlation technique. Optics and Lasers in Engineering. 2008; 46:185–196.
36. Eberl, C.; Thompson, R.; Gianola, DS. Digital Image Correlation and Tracking. 2007. 2006, September 27 ed: http://www.mathworks.com/matlabcentral/fileexchange/12413-digital-image-correlation-and-tracking
37. Jones EMC, Silberstein MN, White SR, Sottos NR. In Situ Measurements of Strains in Composite Battery Electrodes during Electrochemical Cycling. Experimental Mechanics. 2014; 54:971–985.
38. Jones, EMC. Improved Digital Image Correlation (DIC). 2013. 2013, August 14 ed: http://www.mathworks.com/matlabcentral/fileexchange/43073-improved-digital-image-correlation--dic-
39. Schneider CA, Rasband WS, Eliceiri KW. NIH Image to ImageJ: 25 years of image analysis. Nat Methods. 2012; 9:671–5. [PubMed: 22930834]
40. Rasband, W. Image J. Health UNIo; Bethesda, Maryland, USA: 1997–2009.
41. Maas SA, Ellis BJ, Ateshian GA, Weiss JA. FEBio: finite elements for biomechanics. Journal of Biomechanical Engineering. 2012; 134:011005. [PubMed: 22482660]
42. Lu Y, Thiagarajan G, Nicolella DP, Johnson ML. Load/strain distribution between ulna and radius in the mouse forearm compression loading model. Medical Engineering & Physics. 2012; 34:350–356. [PubMed: 21903442]
43. Pfaeffle HJ, Tomaino MM, Grewal R, Xu J, Boardman ND, Woo SL, Herndon JH. Tensile properties of the interosseous membrane of the human forearm. J Orthop Res. 1996; 14:842–5. [PubMed: 8893782]

Highlights

- Study the use of Digital Image Correlation (DIC) to measure strains in mouse bones
- Compare the DIC strain measurements to strain gage readings from ulna and radius
- DIC strain measurements on the bone surfaces exceeded strain gage readings
- Strain gages can stiffen the bone leading to an underestimation of the strain

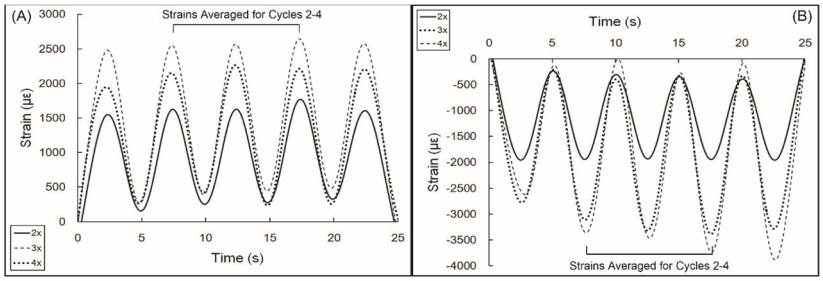

Figure 1.

Representative plots of the strain history in the (A) lateral radius and (B) medial radius for different lens magnifications. Positive peak-to-peak strains denote tension while negative peak-to-peak strains denote compression.

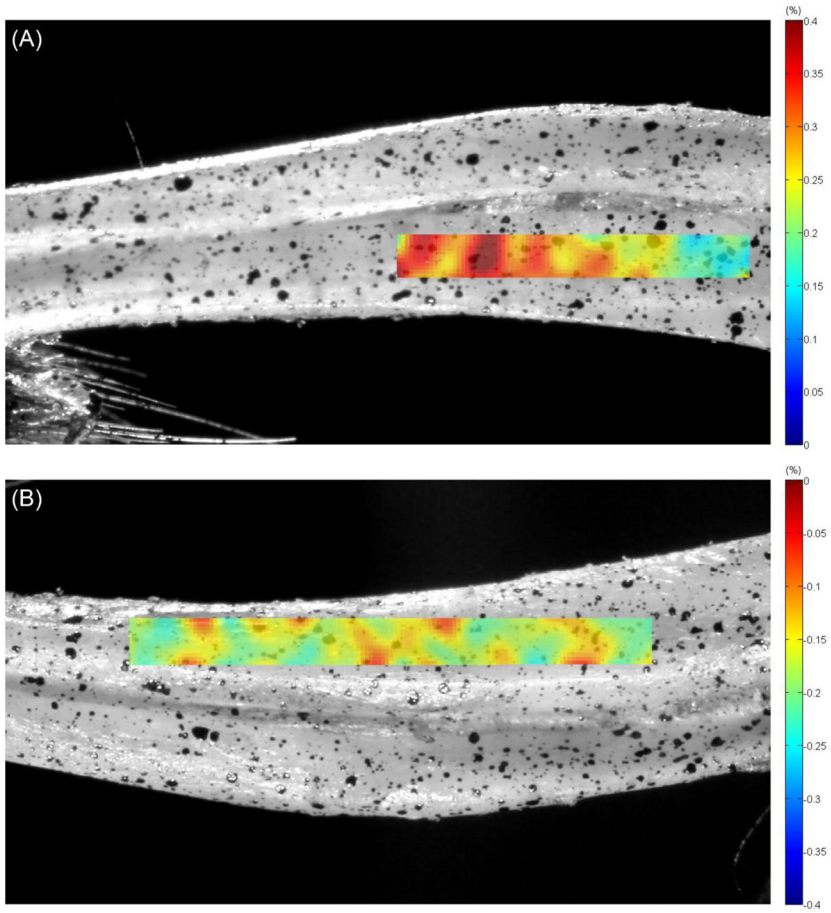

Figure 2.

Representative strain contour plots on the lateral and medial surfaces of the ulna at 1/4 of a loading cycle. The gradient values represent percentages (0.4% = 0.04 strain = 4000 microstrain). (A) The strain contour on the lateral ulna shows a nonuniform tensile strain response. (B) The strain contour on the medial ulna shows a nonuniform compressive strain response.

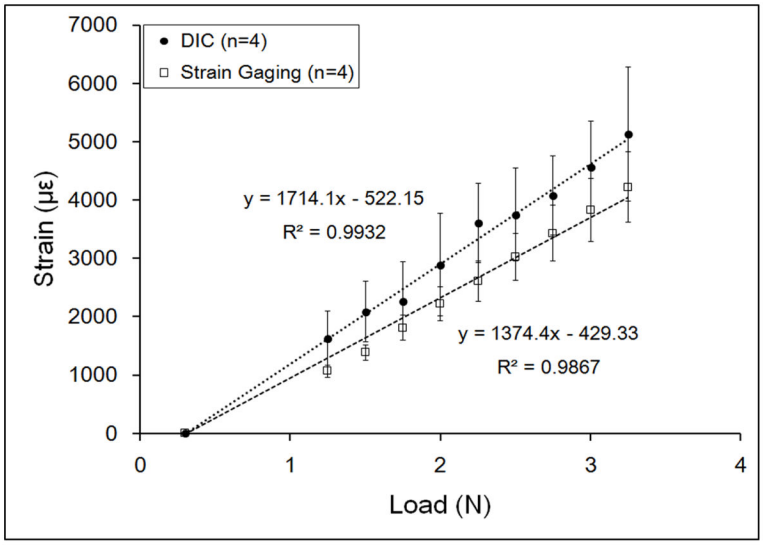

Figure 3.

Load-strain relationships after performing strain gaging and DIC on the medial ulnas of the same set of forearms (*n*=4).

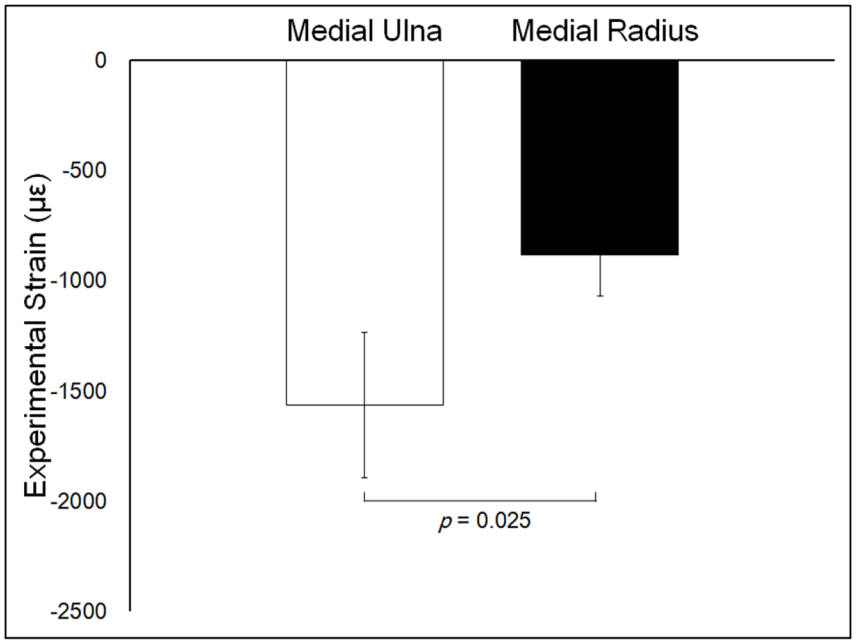

Figure 4.
Comparison of average peak-to-peak strains (Mean ± SD) after strain gaging the medial surface of each bone. Negative strains denote compression.

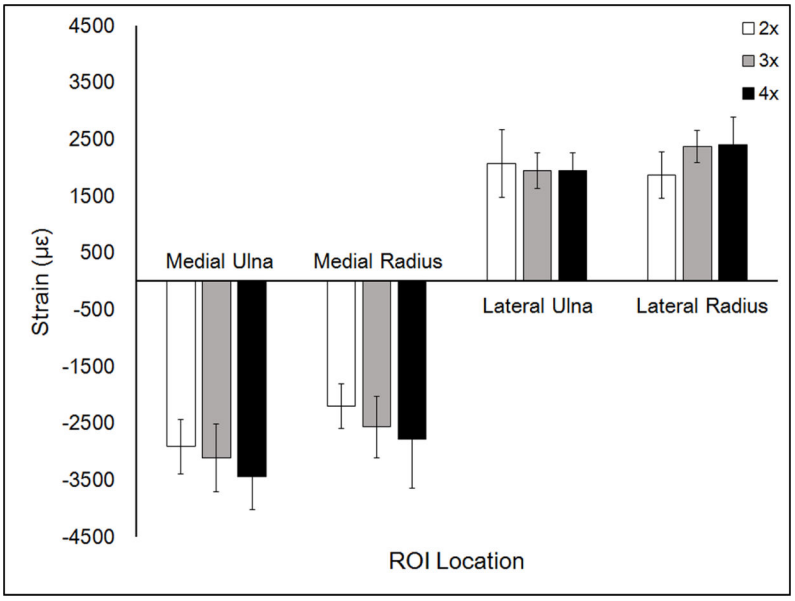

Figure 5.

Comparison of average peak-to-peak strain measurements (Mean ± SD) after performing DIC at different magnifications. Negative strains denote compression while positive strains denote tension.

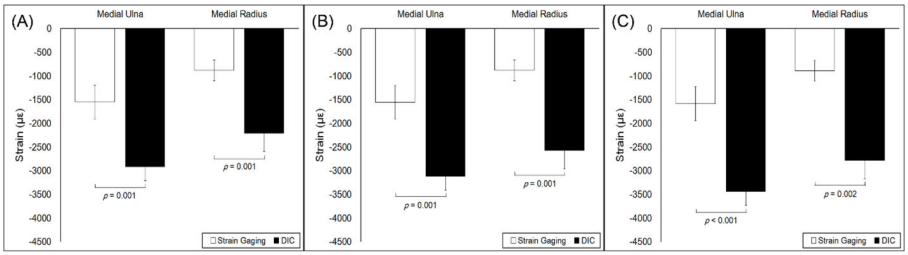

Figure 6.

Comparison of average peak-to-peak strain measurements (Mean ± SD) from strain gaging and DIC at (A) 2x, (B) 3x, and (C) 4x. The significance threshold was set at 0.05, and negative strains denote compression.

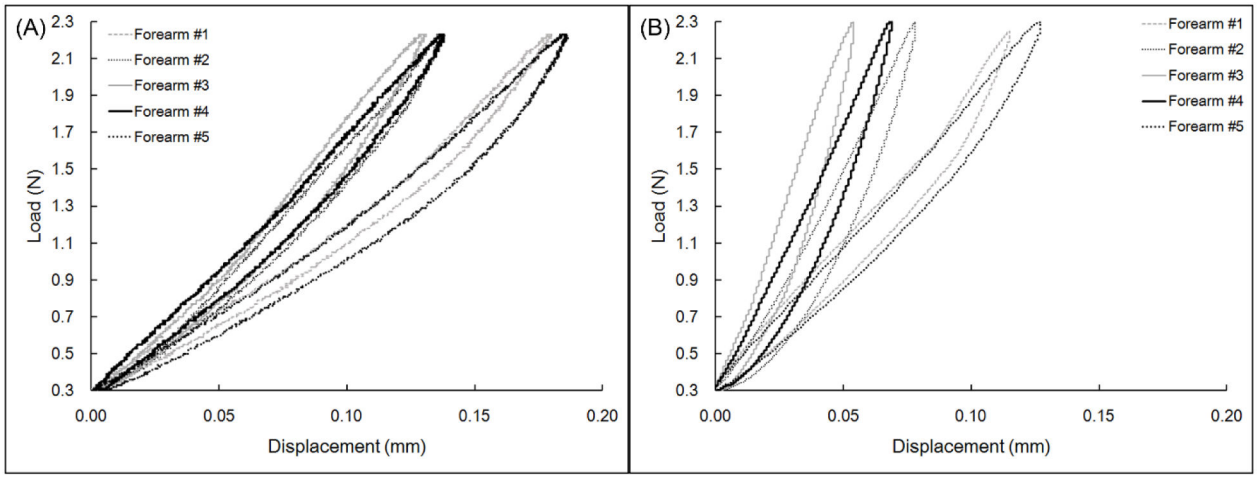

Figure 7.

Load-displacement plots from the same set of forearms (*n*=5) (A) before attaching strain gages and (B) after attaching strain gages.

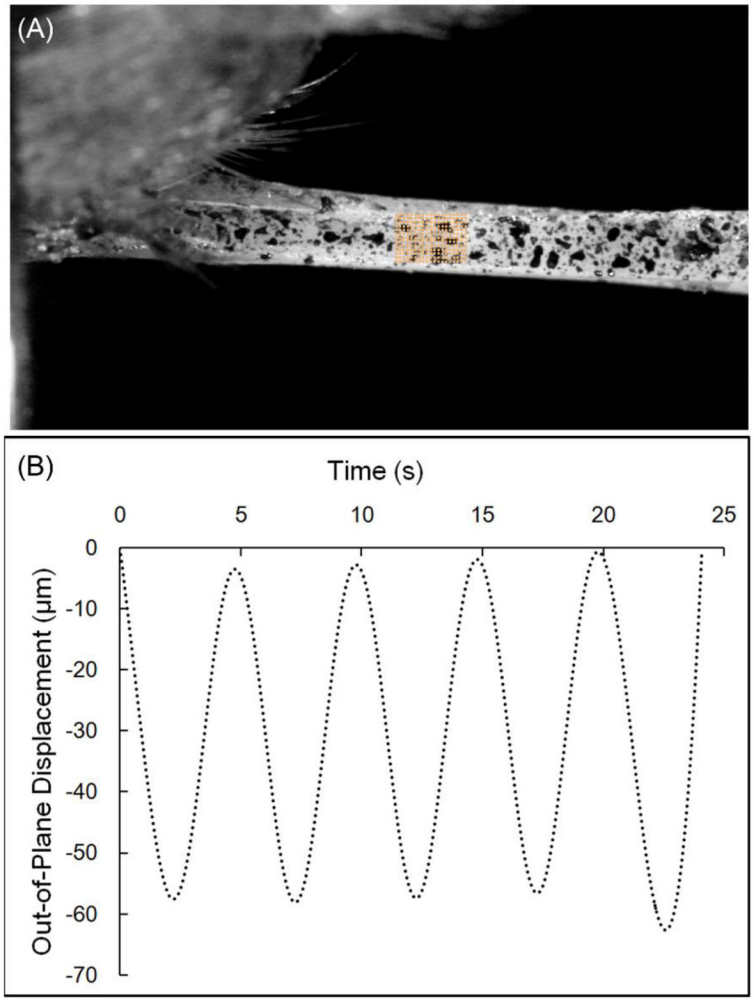

Figure 8.

(A) 4x image of the ulna midshaft and designated ROI after rotating the forearm 90° relative to the original orientation. (B) Representative plot showing the out-of-plane displacement in the radius midshaft due to loading only.

Table 1

Summary of strains due to noise and of their contributions to the total DIC strain measurements.

ROI Location	2x Magnification		3x Magnification		4x Magnification	
	Average Noise (με)	(%) Total DIC Strain	Average Noise (με)	(%) Total DIC Strain	Average Noise (με)	(%) Total DIC Strain
Lateral Radius	79	4.4	46	1.9	54	2.1
Lateral Ulna	53	2.4	71	3.2	93	3.9
Medial Radius	93	3.9	110	4.2	68	2.4
Medial Ulna	81	2.3	70	1.9	92	2.3

Table 2

Summary of stiffness values calculated unloading curves of forearm samples before and after strain gages were attached.

Forearm No.	Stiffness (N/mm) of Unloading Slope	
	Before Strain Gages Attached	After Strain Gages Attached
1	18.7	31.3
2	27.8	46.2
3	23.7	54.9
4	20.0	43.6
5	21.8	27.0

Table 3

Summary of *p*-values showing no significant changes in DIC strain measurements due to changes in lens magnification.

ROI Location	Magnification Comparison	*p*-value
Medial Ulna	2x vs. 3x	0.833
	2x vs. 4x	0.306
	3x vs. 4x	0.589
Medial Radius	2x vs. 3x	0.486
	2x vs. 4x	0.422
	3x vs. 4x	0.940
Lateral Ulna	2x vs. 3x	0.893
	2x vs. 4x	0.871
	3x vs. 4x	0.999
Lateral Radius	2x vs. 3x	0.493
	2x vs. 4x	0.429
	3x vs. 4x	0.993